Mon. Not. R. Astron. Soc. **000**, 000–000 (0000) Printed 1 February 2008 (MN LATEX style file v1.4)

X-ray absorption by ionized oxygen in *ASCA* spectra of the infrared quasar IRAS 13349+2438

W.N. Brandt,[1⋆] S. Mathur,[1] C.S. Reynolds[2] and M. Elvis[1]

[1] *Harvard-Smithsonian Center for Astrophysics, 60 Garden Street, Cambridge, Massachusetts 02138, USA*
[2] *JILA, University of Colorado, Boulder, Colorado 80309-0440, USA*

1 February 2008

ABSTRACT

We present evidence for X-ray absorption by ionized oxygen in *ASCA* spectra of the prototype infrared quasar IRAS 13349+2438. This powerful ($L_{\rm bol} \gtrsim 2 \times 10^{46}$ erg s^{-1}) quasar was studied in detail with *ROSAT*, and the combination of the X-ray data and optical/near-infrared spectropolarimetry strongly suggested the presence of a dusty ionized ('warm') absorber along the line of sight to the central X-ray source. The *ASCA* spectra, in contrast to an earlier claim, show evidence for ionized oxygen edges, and the presence of such edges appears to provide the most physically plausible interpretation of the data. Thus, the *ASCA* spectra support the dusty warm absorber hypothesis. The *ASCA* data also allow the physical properties of the warm absorber to be constrained far better than before. A one-zone warm absorber model indicates the ionized column to be in the range (2–6)$\times 10^{21}$ cm^{-2}, and it gives an ionization parameter of $\xi = 31^{+12}_{-12}$ erg cm s^{-1}. The dusty warm absorber appears to have a density of $\lesssim 3 \times 10^8$ cm^{-3}, and it is probably located outside the broad-line region. The dust in the warm absorber does not appear to have been heavily sputtered or destroyed via other means. Based on the *ASCA* fitting, we suggest that ultraviolet absorption lines from the warm absorber may be detectable and discuss how they can be used to further constrain the warm absorber properties. We compare and contrast the X-ray properties of IRAS 13349+2438 with those of broad absorption line quasars. We comment on the steep > 2 keV continuum of IRAS 13349+2438 and examine the relevance to some models of radiative Fe II formation.

Key words: galaxies: individual: IRAS 13349+2438 – galaxies: active – X-rays: galaxies.

1 INTRODUCTION

IRAS 13349+2438 ($z = 0.107$) is the prototype infrared quasar with high polarization (Beichman et al. 1986; Wills et al. 1992, hereafter W92). It is radio quiet and has a bolometric luminosity of $\gtrsim 2 \times 10^{46}$ erg s^{-1}. W92 presented a detailed model for the optical and near-infrared light paths in IRAS 13349+2438 in which we are viewing the combination of a direct, but attenuated, quasar spectrum and a scattered spectrum. They found an attenuation of at least $E(B-V) = 0.3$, which corresponds to an X-ray absorption column density of $\gtrsim 1.7 \times 10^{21}$ cm^{-2} assuming the mean Galactic dust-to-gas ratio (see equation 7 of Burstein & Heiles 1978). Brandt, Fabian & Pounds (1996, hereafter BFP96) used *ROSAT* Position Sensitive Proportional Counter (PSPC) and Wide Field Camera (WFC) data to test the W92 model. IRAS 13349+2438 was very bright for the PSPC, being seen at up to 5 count s^{-1}. BFP96 found large-amplitude X-ray variability and a high X-ray luminosity which argued against the possibility that most of the X-rays were scattered to Earth around the attenuating matter of W92 (barring an extremely unusual X-ray scattering 'mirror'). Furthermore, they found that the *ROSAT* spectrum constrained the intrinsic X-ray absorption column of neutral matter to be about 35 times smaller than expected based on the optical/near-infrared extinction. To reconcile this large discrepancy, BFP96 invoked a dusty warm absorber, in which the dust causing the optical extinction is embedded in ionized, rather than neutral, gas. This reduced the expected X-ray absorption greatly and thereby allevi-

⋆ Current address: The Pennsylvania State University, Department of Astronomy and Astrophysics, 525 Davey Lab, University Park, Pennsylvania 16802, USA

ated the absorption discrepancy. Fits to the *ROSAT* PSPC spectra showed strong deviations from a simple power-law model. The residuals were consistent with oxygen edges due to absorption by ionized gas, and BFP96 suggested that these might represent a direct detection of the dusty warm absorber. A detailed examination of these features was not possible due to the limited spectral resolution of the PSPC.

The Japanese/USA *ASCA* X-ray satellite (Tanaka, Inoue & Holt 1994) offers improved spectral resolution over *ROSAT* that has allowed detailed studies of ionized oxygen edges in many Seyferts (see Reynolds 1997 for a recent review). Brinkmann et al. (1996) have recently presented the results of an *ASCA* observation of IRAS 13349+2438. They were forced to adopt the dusty warm absorber picture of BFP96 to explain the optical/near-infrared extinction versus cold X-ray column discrepancy. However, one of the main claims of Brinkmann et al. (1996) was that the low-energy *ASCA* spectra ruled out the possibility of ionized oxygen edges between 0.7–1 keV (see their sections 2.2 and 3). Unfortunately, Brinkmann et al. (1996) did not provide any details of the method they used to show that edges were not allowed. If their claim were true, it would be remarkable since it might imply strong temporal variations of the dusty warm absorber of IRAS 13349+2438 (see section 3 of Brinkmann et al. 1996).

In this paper, we carefully examine the strong claim made by Brinkmann et al. (1996) that the *ASCA* spectra are inconsistent with the presence of ionized oxygen edges. Our independent analysis suggests that ionized oxygen edges are, in fact, entirely consistent with the *ASCA* data and provide a highly significant improvement in the quality of fit. They provide a more natural explanation of the low energy spectral complexity than the isolated 0.65 keV line suggested by Brinkmann et al. (1996). Warm absorbers appear to be fairly rare in high luminosity quasars. Since IRAS 13349+2438 is one of the nearest and brightest quasars that shows a warm absorber, it deserves intense study and detailed modelling. We use the *ASCA* data to constrain the warm absorber properties far better than was possible with the *ROSAT* data. We examine the dust-to-gas ratio of the warm absorber as well as the possibility that the warm absorber will imprint absorption lines on the ultraviolet spectrum. We also discuss the unusually steep 2–10 keV continuum slope of IRAS 13349+2438 in the context of what is seen in other strong Fe II, weak [O III], narrow-line Seyfert 1 type galaxies.

We shall adopt $H_0 = 50$ km s^{-1} Mpc^{-1} and $q_0 = \frac{1}{2}$ throughout. The Galactic neutral hydrogen column towards IRAS 13349+2438 has been measured by Murphy et al. (1996), and it is $(1.1 \pm 0.2) \times 10^{20}$ cm^{-2}.

2 OBSERVATIONS AND DATA ANALYSIS

2.1 Observation details

IRAS 13349+2438 was observed twice with *ASCA* during the AO-3 observation round. The observations started on 1995 June 27 and 1995 June 30. Both Solid-state Imaging Spectrometer CCD detectors (SIS0 and SIS1) and both Gas Imaging Spectrometer scintillation proportional counters (GIS2 and GIS3) were operated. The SIS detectors were operated in 1 CCD mode, and the most well-calibrated SIS chips were used (chip 1 for SIS0 and chip 3 for SIS1). The lower level discriminator was not used for the SIS detectors, and this generally facilitates the reliable analysis of data at low energies (K. Mukai, private communication). Both SIS detectors had temperatures in the nominal range [see section 7.2 and section 7.7.3 of the AO-6 *ASCA* Technical Description (AN 97-OSS-02)]. The GIS were operated in PH mode.

We have used the 'Revision 1' processed data from Goddard Space Flight Center (GSFC) for the analysis below (see Day et al. 1995b for a description of Revision 1 processing), and data reduction was performed using FTOOLS and XSELECT (see Day et al. 1995a for a description of these packages and their application to *ASCA* data analysis). We have used the charge transfer inefficiency (CTI) table released on 11 March 1997 [`sisph2pi_110397.fits`; see Dotani et al. 1995 and section 7.7.1 of the AO-6 *ASCA* Technical Description (AN 97-OSS-02) for discussions of CTI]. We have adopted the fairly strict GSFC Revision 1 screening criteria (see Day et al. 1995b), in order to ensure that we are working with data of only the highest quality. After data screening, the exposure times for the first observation are the following: 10.9 ks for SIS0, 10.7 ks for SIS1, and 10.8 ks each for GIS2 and GIS3. After data screening, the exposure times for the second observation are the following: 6.9 ks each for SIS0 and SIS1, and 7.5 ks each for GIS2 and GIS3.

2.2 Image and variability analyses

Our image and variability analyses generally agree with those described by Brinkmann et al. (1996). We shall therefore only describe relevant differences and procedures directly relevant to our spectral analysis below. We use circular source cells centred on IRAS 13349+2438 with radii of 3.5 arcmin and 5 arcmin for SIS and GIS source count extraction, respectively. Due to the position of IRAS 13349+2438 on SIS1 chip 3, our source cell extends slightly past the edge of the chip. There is only a small loss of source counts, and we have verified that this is not materially affecting the spectral results below by using several smaller source cell sizes and comparing the derived results. We have carefully chosen local, circular, source-free cells to use for background subtraction. We have chosen our GIS background cells so that they lie at similar distances from the centres of the detectors as IRAS 13349+2438. We use the counts extracted from these cells in all analysis below.

We confirm the rapid X-ray variability found by Brinkmann et al. (1996). The count rate appears to rise by about 50 per cent in ≈ 6000 s near the end of the first observation. This variability is quite rapid for a quasar with a bolometric luminosity of $\gtrsim 2 \times 10^{46}$ erg s^{-1}. For example, if the predominant fraction of the observed bolometric luminosity is ultimately due to accretion onto a Kerr black hole radiating at 20 per cent of the Eddington limit, the variability timescale is comparable to the light crossing timescale of the 8×10^8 M$_\odot$ black hole. The required accretion efficiency, in the absence of relativistic effects, is reasonably high (~ 3 per cent) but not outstanding (here we use the arguments of Fabian 1979). The rapid X-ray variability seen by *ASCA* is entirely consistent with the idea that we are seeing X-rays directly from the quasar core (see section 4.2 of BFP96 for further discussion).

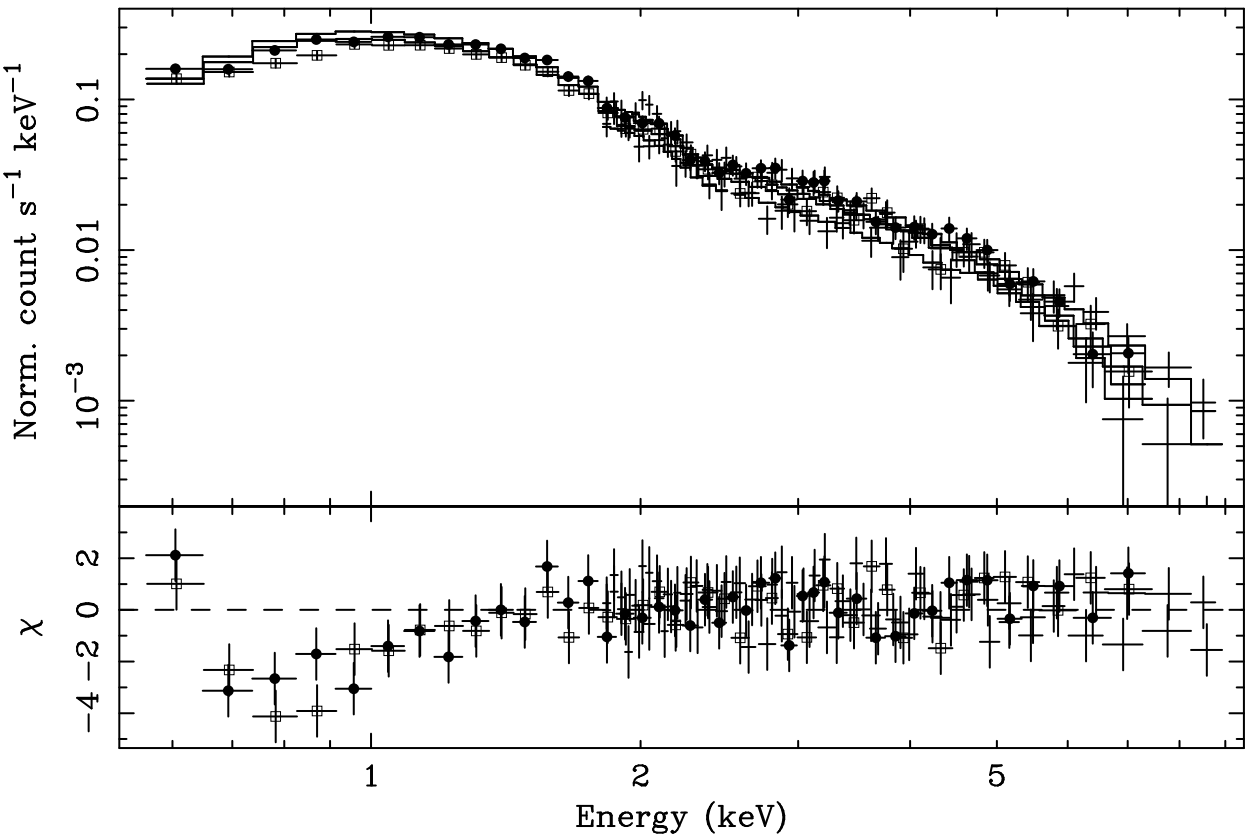

Figure 1. *ASCA* SIS0 (solid dots), SIS1 (open squares) and GIS (plain crosses) spectra of IRAS 13349+2438. A power-law model has been fit to the data above 2 keV and then extrapolated back to show the deviations from a power-law model at low energies. The ordinate for the lower panel (labeled χ) shows the fit residuals in terms of sigmas with error bars of size one. Note the systematic residuals at low energies due to absorption edges from ionized oxygen. This spectrum is in the observed frame, so the 0.739 keV O VII K-edge threshold is redshifted to 0.668 keV.

As in Brinkmann et al. (1996), no highly significant spectral variability is detected. Brinkmann et al. (1996) state that the current *ROSAT* and *ASCA* data demonstrate that IRAS 13349+2438 varies achromatically across the entire 0.1–8 keV range. The data are indeed consistent with this possibility. However, the *ROSAT* and *ASCA* observations were not simultaneous. It is still entirely possible then that the 0.1–0.5 keV spectrum (e.g. a soft X-ray excess) varies independently relative to the 0.5–8 keV spectrum.

2.3 Spectral analysis

2.3.1 Preparation of spectra and fitting details

We have extracted spectra from each detector using all of the acceptable exposure time. As no spectral variability is evident, we have combined the 1995 June 27 and 1995 June 30 data. IRAS 13349+2438 is detected up to ≈ 7.5 keV by the SIS detectors, and it is detected up to ≈ 9.0 keV by the GIS detectors. In the rest frame of IRAS 13349+2438, these upper detection energies correspond to ≈ 8.3 keV and ≈ 10.0 keV, respectively. We have grouped the 0.55–7.5 keV SIS spectra and the 1–9 keV GIS spectra so that there are 12 photons per spectral data point, to allow the use of chi-squared fitting techniques. Following the suggestions of the GSFC *ASCA* guest observer facility, we have used the SISRMG software to generate our SIS redistribution matrix files (rmf), and we use the GIS rmf from 1995 March 6. We generate our ancillary response files (arf) using the ASCAARF software. We perform spectral modelling below using the X-ray spectral models in the XSPEC spectral fitting package (Shafer et al. 1991; Arnaud 1996). Unless stated otherwise, we shall conservatively quote errors for 90.0 per cent confidence taking all parameters to be of interest other than absolute normalization.

We first performed spectral fitting for each of the *ASCA* detectors separately, and we obtained results that were consistent to within the errors. We have therefore jointly fitted

the spectra from all four detectors, and we detail these results below. In such joint fitting we allow the normalization for each detector model to be free (to allow for small calibration uncertainties in the absolute normalizations between detectors; this is currently standard practice when performing *ASCA* analysis), but we tie together all other fit parameters across the four *ASCA* detectors. When we quote fluxes below, we shall quote them for the SIS0 detector.

2.3.2 Spectral fitting results

We have fitted the spectra described above with a simple power-law model. We obtain $N_{\rm H} = (2.55^{+2.89}_{-2.25}) \times 10^{20}$ cm^{-2}, $\Gamma = 2.19^{+0.08}_{-0.07}$ and $\chi^2 = 543.1$ for 632 degrees of freedom ($\chi^2_\nu = 0.859$). The fit is formally acceptable, although it leaves systematic residuals in the 0.55–1.0 keV range. The residuals are systematically above the fit in the $\approx$ 0.55–0.65 keV band, and they are systematically below the fit in the $\approx$ 0.65–1.0 keV band (see below for further discussion). The fitted neutral absorption column is consistent with the Galactic value and that measured by the *ROSAT* PSPC. Indeed, *ROSAT* PSPC fitting showed the cold column intrinsic to IRAS 13349+2438 was $< 5 \times 10^{19}$ cm^{-2} (see section 4.1 of BFP96). Therefore, from this point on, we shall adopt the Galactic neutral absorption column unless stated otherwise. Performing a power-law fit with the column fixed to the Galactic value, we obtain $\Gamma = 2.17^{+0.04}_{-0.04}$ and $\chi^2 = 545.4$ for 633 degrees of freedom ($\chi^2_\nu = 0.862$).

In order to investigate the systematic 0.55–1.0 keV residuals further, we have fitted a power-law model to the data in the 2–10 keV band (corrected for redshift) and then extrapolated this model down to lower energies. In the 2–10 keV band, we obtain a photon index of $\Gamma = 2.22^{+0.08}_{-0.08}$. The fit quality is good with $\chi^2 = 311.8$ for 408 degrees of freedom ($\chi^2_\nu = 0.764$), and there are no obvious systematic residuals in the 2–10 keV range. Upon extrapolation of this model to lower energies, negative residuals are clearly apparent in the 0.65–1.3 keV band (see Figure 1). Such residuals are frequently seen in *ASCA* data when ionized absorbing matter lies along the line of sight (compare our Figure 1 with figure 3 of Reynolds 1997), and they are attributed to the presence of edges due to ionized oxygen in the X-ray spectrum. In order to examine possible oxygen absorption in the spectrum of IRAS 13349+2438, we have first added an edge to the power-law model from the previous paragraph. We obtain $\Gamma = 2.27^{+0.07}_{-0.07}$, $E_{\rm Edge} = 0.75^{+0.04}_{-0.04}$ keV, $\tau_{\rm Edge} = 0.41^{+0.14}_{-0.13}$ and $\chi^2 = 517.4$ for 631 degrees of freedom ($\chi^2_\nu = 0.819$; the edge parameter errors are quoted for $\Delta\chi^2 = 2.71$ and the edge threshold energy has been corrected for redshift). The fit quality is good, and the low energy systematic residuals described in the previous paragraph are removed. We show confidence contours for the edge parameters in Figure 2. The edge energies usually seen in Seyfert ionized absorbers are 0.739 keV for the O VII K edge and 0.871 keV for the O VIII K edge. Our best fitting edge energy lies between these two values. It is in good agreement with the O VII K edge energy, which is the strongest edge usually seen in warm absorbers. Applying the F-test (see tables C-5 and C-6 of Bevington & Robinson 1992) with $\Delta\chi^2 = -28.0$ for the two additional edge parameters, we find that the addition of the edge makes a significant improvement to the fit quality with over 99 per cent confidence. We have tried adding edges at other arbitrary energies from 1.0–2.5 keV, and none reduces the value of χ^2 enough that it makes a highly significant improvement to the fit quality (this helps to validate the significance of our F-test results).

We have also modelled the residuals using two edges with their threshold energies fixed at the 0.739 keV (Edge 1) and 0.871 keV (Edge 2) threshold energies for O VII and O VIII. We obtain $\Gamma = 2.28^{+0.07}_{-0.07}$, $\tau_{\rm Edge\ 1} = 0.37^{+0.15}_{-0.15}$, $\tau_{\rm Edge\ 2} = 0.09^{+0.11}_{-0.09}$ and $\chi^2 = 515.8$ for 631 degrees of freedom ($\chi^2_\nu = 0.817$; the errors for the edge depths are for $\Delta\chi^2 = 2.71$). Applying the F-test with $\Delta\chi^2 = -29.6$ for the two additional edge parameters, we again find a highly significant improvement with over 99 per cent confidence (as compared to the simple power-law model). We cannot statistically discriminate between the one-edge model of the previous paragraph and the two-edge model discussed here. Based on *ASCA* observations of nearby Seyferts, we suspect that the two-edge model is the most physically appropriate.

We have verified that potential calibration uncertainties at low energies do not appear to be affecting the basic nature of our results. Dotani et al. (1996) have examined calibration systematics in this energy range and find that they are $\approx$ 10 per cent or less (see their section 2.3). We comment that we are using the data in the 0.55–0.6 keV band only for the purpose of defining the basic continuum level below the edge. This use of the 0.55–0.6 keV data requires somewhat less of the calibration than does, for example, precision X-ray emission line work in this energy range (see George, Turner & Netzer 1995 who examine a possible O VII emission line at 0.57 keV). If we completely ignore the data in the 0.55–0.6 keV band we obtain the same qualitative results. In this case, the addition of two edges with their threshold energies fixed at 0.739 keV and 0.871 keV gives $\Delta\chi^2 = -21.1$ for two additional parameters (relative to a simple power-law model). The F-test indicates that this is a significant improvement in χ^2 with over 99 per cent confidence.

To model our data more realistically, we have fitted the *ASCA* spectrum with a one-zone warm gas absorption model constructed from CLOUDY (Ferland 1992) calculations. The model is the same as that described in section 3.1 of Reynolds et al. (1995), and line emission from the warm absorber is consistently included assuming a covering fraction of unity for the warm absorber (even for unity covering fraction, the lines are quite small for the range of physical parameters under consideration here and do not substantially affect the fitting given the statistics of these *ASCA* data). This model gives a good fit with $\chi^2 = 518.6$ for 631 degrees of freedom. The derived fit parameters are $\Gamma = 2.31^{+0.07}_{-0.15}$, $\log(N_{\rm H,warm}) = 21.59^{+0.15}_{-0.26}$ and $\xi = 31.4^{+12.1}_{-12,2}$ erg cm s^{-1} (warm absorber parameter errors are for $\Delta\chi^2 = 2.71$). The ionization parameter, ξ, is defined to be $L/(nR^2)$ where L is the ionizing luminosity, n is the number density of the absorbing plasma and R is the distance to the illuminating source. Relative to the simple power-law model we obtain $\Delta\chi^2 = -26.8$. The F-test indicates that the one-zone warm absorber model makes a significant improvement in fit quality with over 99 per cent confidence. The fit quality is not quite as good as that for just two simple edges, although there is no statistically significant difference.

We have used the power-law and one-zone warm absorber model to compute mean fluxes and the mean luminosity in the 2–10 keV band. The absorbed and absorption-

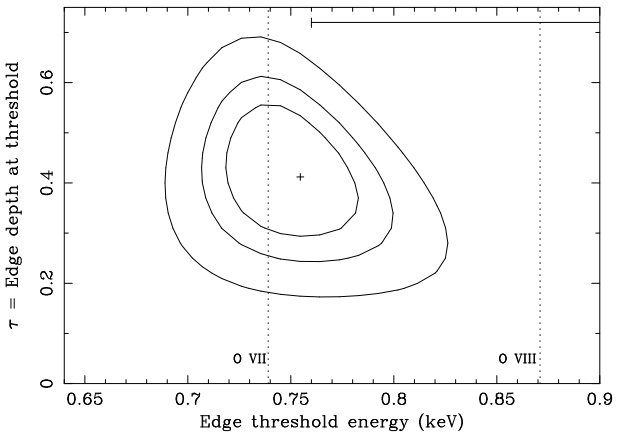

Figure 2. *ASCA* confidence contours for the edge parameters. Contour levels are for $\Delta\chi^2 = 2.30$ (inner contour; 68.3 per cent confidence for two parameters of interest), $\Delta\chi^2 = 4.61$ (middle contour; 90.0 per cent confidence for two parameters of interest) and $\Delta\chi^2 = 9.21$ (outer contour; 99.0 per cent confidence for two parameters of interest). The fitted edge energy has been corrected for cosmological redshift. The threshold energies for the O VII K edge (0.739 keV) and the O VIII K edge (0.871 keV) are shown as vertical dotted lines. The lower part of the edge threshold energy range derived from *ROSAT* data is shown as the horizontal solid line at the top of the figure (the y-axis position of the line is arbitrary). Note that the derived edge energy from the *ASCA* fitting is in good agreement with with the threshold energy for the O VII K edge. This is the strongest edge usually seen in Seyfert warm absorbers.

corrected 2–10 keV fluxes are both 5.7×10^{-12} erg cm^{-2} s^{-1}, and the derived 2–10 keV isotropic luminosity is 3.0×10^{44} erg s^{-1}. We have also used the same model to compute mean fluxes and the mean luminosity in the 0.55–2 keV band. The absorbed and absorption-corrected 0.55–2 keV fluxes are 6.0×10^{-12} erg cm^{-2} s^{-1} and 7.0×10^{-12} erg cm^{-2} s^{-1}, respectively. The derived 0.55–2 keV isotropic luminosity is 3.6×10^{44} erg s^{-1}. Fluxes and luminosities derived using the models with simple edges described above are very similar to those quoted here.

Finally, we have fitted the 3–10 keV data (corrected for redshift) with a simple power-law model to look for any evidence of continuum curvature. We obtain an acceptable fit and a photon index of $2.20^{+0.16}_{-0.17}$. There is no significant evidence for continuum curvature (i.e. the 2–10 keV and 3–10 keV photon indices are consistent with each other) although the constraints are not tight.

2.3.3 Safety checks

Due to the fact that our results regarding the presence of oxygen edges are in contradiction to the claims of Brinkmann et al. (1996), we have repeated our analysis in several ways to ensure its reliability. Data analysis has been performed independently by three of the authors (WNB, SM, CSR) using *ASCA* software installations at two different institutions, and all results are in generally good agreement. We have repeated our analysis using the 1994 November 9 SIS rmf files, and using these does not materially change our conclusions. We have also repeated our analysis using the GSFC blank sky fields for background subtraction, and the use of these does not change our conclusions. If we use older CTI tables (see Section 2.1) the agreement between SIS0 and SIS1 is not as good, but oxygen edges still provide a reduction in χ^2 that is significant with over 99 per cent confidence.

Additional spectral fitting by Y. Ogasaka (who was primarily responsible for the *ASCA* analysis presented in Brinkmann et al. 1996) now also shows that oxygen edges are entirely consistent with the actual Brinkmann et al. (1996) spectra (Y. Ogasaka, private communication).

3 DISCUSSION

3.1 Spectral features from warm absorption

3.1.1 Oxygen edges in the ASCA spectra

We find that the presence of ionized oxygen edges is entirely consistent with the *ASCA* spectra of IRAS 13349+2438. The addition of ionized oxygen absorption provides a highly significant improvement in χ^2, and the derived energy range for the absorption comes out to be in good agreement with that seen from O VII and O VIII in many other Seyfert 1 class objects. While we cannot statistically prove that oxygen edges are the only possible interpretation of the low-energy residuals (a fairly common situation in X-ray data analysis), such absorption is expected due to the large optical/near-infrared extinction versus cold X-ray column discrepancy established for IRAS 13349+2438 (BFP96). An *isolated* oxygen emission line at 0.65 keV, as proposed by Brinkmann et al. (1996), has not been seen in other Seyfert 1 class objects to our knowledge (IRAS 13349+2438 should be treated as a Seyfert 1 class object in this context due to the fact that its X-ray variability demonstrates that we are seeing the X-ray continuum directly from its black hole region). While low-energy oxygen emission lines have been claimed in some Seyfert 1s (e.g. George et al. 1995), they are thought to be associated with warm absorbers and have been seen to be accompanied by much stronger oxygen edge features. An isolated oxygen line could perhaps arise if there were line-emitting warm absorber type gas out of the line of sight but not along the line of sight. However, as noted above, we have good, independent reasons to think that a warm absorber in IRAS 13349+2438 lies along the line of sight. While, of course, some contribution to the *ASCA* residuals is probably due to oxygen line emission (indeed, this is required by atomic physics provided the ionized gas subtends a non-negligible solid angle), it seems most plausible that the dominant contribution is due to oxygen absorption edges. It is difficult to pinpoint the precise origin of our disagreement with Brinkmann et al. (1996), as they present insufficient details of the analysis behind their strong claim that edges in the 0.7–1.0 keV range are inconsistent with the *ASCA* data. Instead we have established that oxygen edges are in good statistical agreement with the *ASCA* data and moreover provide a physically plausible explanation for the observed residuals.

3.1.2 ASCA warm absorber constraints

The *ASCA* data provide much more reliable warm absorber constraints than the *ROSAT* data. The limited spectral resolution of *ROSAT* can make fitting constraints on warm absorbers difficult to obtain. *ROSAT* fitting with an edge model gave a rather high edge energy of $0.86^{+0.10}_{-0.10}$ keV although the statistical error bar was also large (compare with Figure 2). BFP96 clearly discussed the difficulties of precision modelling of the warm absorber using *ROSAT* data. In particular, there is probably a soft excess in the low-energy end of the *ROSAT* band which affects the fitted *ROSAT* warm absorber parameters due to the limited spectral resolution of the PSPC (see section 3.3 of BFP96).

Fitting the one-zone warm absorption model to the *ASCA* data indicates the ionized column along the line of sight is $\approx$(2–6)$\times10^{21}$ cm^{-2}, which is rather similar to that seen in many less luminous Seyferts. The fitted *ASCA* warm column is smaller than the *ROSAT* warm column of $\log(N_{\rm H,warm}) = 22.78^{+1.20}_{-1.18}$, although the two measured values are not formally discrepant. The *ASCA* errors on the column are about 4 times smaller than the *ROSAT* errors. W92 argue the extinction to the nucleus of IRAS 13349+2438 has $E(B-V)$ in the range 0.3–0.7 (see their section 4.4.3). Using the mean Galactic dust-to-gas ratio, the gas column range that corresponds to this $E(B-V)$ range is (1.7–4.0)$\times10^{21}$ cm^{-2}. The good agreement of the fitted *ASCA* warm column range with this range is remarkable, given the very different environments under consideration (i.e. the local interstellar medium as compared to ionized gas around a quasar). Provided the one-zone warm absorption modelling is roughly appropriate, it appears likely that the dust in the warm absorber of IRAS 13349+2438 has not been heavily sputtered or destroyed via other means. Given the apparent lack of heavy sputtering, equation 44 of Draine & Salpeter (1979) suggests that the temperature of the ionized gas must be less than about 10^6 K provided its density is $\gtrsim 5\times10^4$ cm^{-3} (also see section VI of Burke & Silk 1974, who quote a somewhat lower sputtering threshold temperature). Collisionally ionized gas with O VII and O VIII would have a temperature of $\gtrsim 10^6$ K (see table 3 of Shull & Van Steenberg 1982), so it seems unlikely that the warm absorber gas is collisionally ionized. This appears to vindicate our implicit assumption of photoionization.

The *ASCA* ionization parameter is 4.6 times lower than and inconsistent with the value of $\xi = 145^{+80}_{-56}$ erg cm s^{-1} derived from the *ROSAT* data. The *ASCA* error bars are again much smaller than the *ROSAT* error bars. The *ASCA* ionization parameter is in better agreement with what is usually seen in Seyfert 1 class objects (compare with table 6 of Reynolds 1997). Adding a soft excess to the *ROSAT* data (see above) allows for consistency between the *ROSAT* and *ASCA* warm absorber parameters, although the *ROSAT* parameters are very poorly constrained. In addition, of course, there may well have been significant warm absorber variability in the $\sim$ 3 years between the *ROSAT* and *ASCA* observations.

Given the ionization parameter of the warm absorber and the fact that it contains dust, we can derive an upper limit on its density. We have the relation $n = L/\xi R^2$ (see Section 2.3.2 for the definitions of the symbols). From the *ASCA* fitting we have $\xi \approx 31$ erg cm s^{-1}, and from the observed *ROSAT* and *ASCA* luminosities we derive a mean ionizing luminosity of $\approx 1.5\times10^{45}$ erg s^{-1}. In order to avoid sublimation the dust must be $\gtrsim 4\times10^{17}$ cm from the nucleus (see section 5.3 of Laor & Draine 1993). Thus we derive $n \lesssim 3\times10^8$ cm^{-3}, which is significantly less than the density of a typical cloud in the broad-line region. The dusty warm absorber of IRAS 13349+2438 is probably located outside its broad-line region, perhaps in its intermediate-line region or narrow-line region. We also comment that if the warm absorber gas is above the dust sputtering threshold temperature, then the apparent lack of heavy sputtering can be used to derive stringent constraints on the warm absorber density (see equation 35 of Burke & Silk 1974 and equation 44 of Draine & Salpeter 1979).

An observation with *AXAF*, or even a longer observation with *ASCA* (note the total exposure time for these two observations was rather short), would allow further constraints to be placed on the dusty warm absorber. It would be especially interesting to study warm absorber variability and to better constrain the radial velocity of the X-ray absorbing gas. The agreement between the fitted *ASCA* edge energy and the O VII K-edge threshold energy suggests that the warm absorber is moving at less than about 6 per cent of the speed of light.

3.1.3 UV absorption lines — constraints, predictions and relevance to broad absorption line quasars

In several active galaxies, ionized X-ray absorption may well be associated with ultraviolet absorption lines (e.g. Mathur, Elvis & Wilkes 1995 and references therein). To investigate whether this is the case for IRAS 13349+2438, we have looked for ultraviolet absorption lines in the *International Ultraviolet Explorer (IUE)* spectrum from Lanzetta, Turnshek & Sandoval (1993). No strong lines are seen in the spectrum from the SWP instrument, but it is fairly noisy and strong line constraints are not available from these data. The absorption feature at $\approx$ 3050 Å near the Mg II emission line in the spectrum from the LWP instrument is most probably an instrumental reseaux mark (see figure 2 of Kolman et al. 1992).

Ionization fractions of ions ($f_{\rm ion}$) like O VI, C IV and N V can be determined for a given ionization parameter (see figure 4 in Mathur, Wilkes and Aldcroft 1997 for $f_{\rm ion}$ as a function of ionization parameter). The best-fit value of the ionization parameter of the warm absorber in IRAS 13349+2438 is $\xi = 31.4$ (corresponding to $U \sim 1.3$ for a standard active galactic nucleus continuum as defined in CLOUDY). The absorbing column density in each ion is then $N_{\rm ion} = N_{\rm H,warm} \times f_{\rm ion} \times A_{\rm element}$ where $A_{\rm element}$ is the abundance of the element relative to hydrogen. In the warm absorber of IRAS 13349+2438, the C IV and N V absorption line column densities are expected to be $\gtrsim 10^{16}$ cm^{-2} while the column density in O VI would be $\gtrsim 7\times10^{17}$ cm^{-2}. We thus expect to see high ionization absorption lines of O VI, C IV, N V and Lyα in high quality ultraviolet spectra of IRAS 13349+2438. Note, however, that if the ionization parameter is towards the higher end of the range allowed by the *ASCA* fitting, the expected column densities would be significantly lower. Spectra from the *Hubble Space Telescope* would allow the ionization state of the dusty warm absorber

to be further constrained. If lines are detected, they might also constrain its velocity along the line of sight.

High-quality ultraviolet spectra are also important to obtain for IRAS 13349+2438 due to its high polarization and its radio-quiet nature. Almost all highly-polarized, radio-quiet quasars are thought to be broad absorption line (BAL) quasars, and so it would be interesting to know if IRAS 13349+2438 is a BAL quasar as well. IRAS 13349+2438 has the strong optical Fe II emission, weak [O III] emission and strong far-infrared emission that are typical of low-ionization BAL quasars (e.g. section 3.2 of Boroson & Meyers 1992). BAL quasars are generally known to be weak soft X-ray emitters, and this is probably due to heavy X-ray absorption in their nuclei (see Green & Mathur 1996 and references therein). Their small soft X-ray fluxes have made them elusive X-ray sources, and to date there is no confirmed BAL quasar with a high-quality X-ray spectrum (i.e. one that allows both the column density and ionization state of the absorbing matter to be determined with reasonable precision by X-ray spectral fitting). In sharp contrast to the general situation for BAL quasars, IRAS 13349+2438 is a strong soft X-ray source and was one of the brightest active galaxies in the *ROSAT* sky. It appears to have much less X-ray absorption than is often seen in BAL quasars. If ultraviolet spectra do show IRAS 13349+2438 to be a BAL quasar, then it will be the first BAL quasar with a high-quality X-ray spectrum. IRAS 13349+2438 might represent an intermediate object between BAL quasars and other quasars with associated absorption systems. It may be oriented such that our line of sight to the central X-ray source only skims the surface of the BAL outflow. We might then only be looking through an ionized surface layer of the outflow. Finally, some models for BAL outflows suggest that they are accelerated by radiation pressure on dust (see section 3.3 of de Kool 1997 for a review). The fact that we find evidence for dusty, ionized gas in IRAS 13349+2438 may lend observational support to such models.

3.2 The steep hard X-ray continuum

The *ASCA* data show the 2–10 keV spectrum of IRAS 13349+2438 to be unusually steep with $\Gamma \approx 2.22$. Comparing this photon index with the photon index distributions shown in figure 10 of Nandra et al. (1997) and figure 2 of Reynolds (1997) makes this clear, as IRAS 13349+2438 is steeper than all of these objects except for Mrk 766. Mrk 766 is a narrow-line Seyfert 1 galaxy (see Osterbrock & Pogge 1985; Goodrich 1989; Boller, Brandt & Fink 1996) that has been claimed to have strong photon index variability by Leighly et al. (1996).

BFP96 compared the properties of IRAS 13349+2438 to those seen in many narrow-line Seyfert 1s, and they found a striking number of similarities including strong Fe II, weak [O III], relatively narrow permitted line cores (with FWHM of ≈ 2100 km s^{-1}), a relatively soft X-ray spectrum and rapid X-ray variability for an object of its luminosity (see their section 4.5 and compare with the primary eigenvector of Boroson & Green 1992). Brandt, Mathur & Elvis (1997) have systematically compared the 2–10 keV *ASCA* power-law slopes of soft *ROSAT* narrow-line Seyfert 1s to those of Seyfert 1s with larger Hβ FWHM values. They found that soft *ROSAT* narrow-line Seyfert 1s as a class appear to have generally steeper 2–10 keV power-law slopes (they also pointed out that some soft *ROSAT* narrow-line Seyfert 1s may have interesting 2–10 keV continuum curvature). IRAS 13349+2438 appears to follow the hard photon index trend seen in many narrow-line Seyfert 1s, further strengthening the comparisons made in section 4.5 of BFP96. In addition, the rapid X-ray variability seen by *ASCA* adds to the similarity.

The steep 2–10 keV slopes of IRAS 13349+2438 and some other strong optical Fe II emitters (e.g. I Zwicky 1) in Brandt et al. (1997) have implications for models of radiative Fe II formation. While some narrow-line Seyfert 1s may have interesting 2–10 keV continuum curvature (see Brandt et al., in preparation), none has shown evidence for a spectral flattening to a slope less than those of typical Seyfert 1s. Therefore, in the absence of any strong spectral flattening above the *ASCA* band, their hard X-ray emission will be comparatively weak. This provides evidence against models of optical Fe II line formation that require very flat hard X-ray spectra and strong hard X-ray emission (e.g. the Compton-heating model of Collin-Souffrin, Hameury & Joly 1988; see the last paragraph of their section 4). While this does not settle the debate as to whether optical Fe II is formed in a mechanically heated or radiatively heated medium, it does argue against one radiative heating model. Other radiative heating models predict an anticorrelation between Fe II/Hβ and hard X-ray luminosity (see section 4 of Joly 1993 and references therein), and this appears to be what the currently available X-ray data suggest. Further *ASCA* and *SAX* measurements of the hard X-ray spectra of strong optical Fe II emitters (e.g. PHL 1092, Mrk 42 and Mrk 957) will provide additional constraints, and such observations are planned.

4 SUMMARY

We have analysed and interpreted the *ASCA* data for the prototype infrared quasar IRAS 13349+2438. Our main results are the following:

(1) The *ASCA* spectra show systematic deviations from a power-law model in the 0.55–1 keV band. The addition of K edges from O VII and O VIII removes the systematic deviations and provides a highly significant improvement in fit quality. The *ASCA* evidence for oxygen absorption is consistent with the dusty warm absorber hypothesis put forward based on *ROSAT* and optical/near-infrared data.

(2) The *ASCA* data greatly improve the X-ray constraints on the warm absorber. Fitting a one-zone warm absorber model gives an ionized column of $(2\text{–}6)\times10^{21}$ cm^{-2} and an ionization parameter of $\xi = 31^{+12}_{-12}$ erg cm s^{-1}. Assuming the mean Galactic dust-to-gas ratio, the ionized column and the column expected from the $E(B-V)$ measurement are in good agreement. The dusty warm absorber is probably located outside the broad-line region and has a number density $\lesssim 3\times10^{8}$ cm^{-3}.

(3) We use the *ASCA* data to make predictions about ultraviolet absorption in the context of the unified ultraviolet/X-ray absorber model. Many properties of IRAS 13349+2438 are similar to those seen in broad absorption line quasars, but in contrast to many broad absorption line quasars IRAS 13349+2438 is bright in the soft X-ray band. If IRAS 13349+2438 is a broad absorption line

quasar, then it is the first one with a high-quality X-ray spectrum.

(4) The 2–10 keV spectrum of IRAS 13349+2438 is steep ($\Gamma = 2.22^{+0.08}_{-0.08}$). This and other properties of IRAS 13349+2438 resemble those seen in narrow-line Seyfert 1 galaxies. We discuss the relevance of the steep 2–10 keV slope to some models of radiative Fe II formation.

ACKNOWLEDGMENTS

We gratefully acknowledge financial support from the Smithsonian Institution (WNB), NASA grant NAG5-3249 (SM), NSF grant AST-9529175 (CSR) and NASA grant NAG5-3066 (ME). We thank J.P. Halpern, Y. Ogasaka, B.J. Wilkes and B.J. Wills for helpful discussions. We thank K. Mukai and R.F. Mushotzky for advice regarding *ASCA* calibration issues. We thank the members of the *ASCA* team who have made these observations possible.

REFERENCES

Arnaud K.A., 1996, in Jacoby G., Barnes J., eds, Astronomical Data Analysis Software and Systems V: ASP Conference Series # 101. ASP Press, San Francisco, p. 17
Beichman C.A., Soifer B.T., Helou G., Chester T.J., Neugebauer G., Gillett F.C., Low F.J., 1986, ApJ, 308, L1
Bevington P.R., Robinson D.K., 1992, Data Reduction and Error Analysis for the Physical Sciences: Second Edition. McGraw Hill, New York
Boller Th., Brandt W.N., Fink H., 1996, A&A, 305, 53 (BBF96)
Boroson T.A., Green R.F., 1992, ApJS, 80, 109
Boroson T.A., Meyers K.A., 1992, ApJ, 397, 442
Brandt W.N, Fabian A.C., Pounds K.A., 1996, MNRAS, 278, 326 (BFP96)
Brandt W.N., Mathur S., Elvis M., 1997, MNRAS, 285, L25
Brinkmann W., Kawai N., Ogasaka Y., Siebert J., 1996, A&A, 316, L9
Burke J.R., Silk J., 1974, ApJ, 190, 1
Burstein D., Heiles C., 1978, ApJ, 225, 40
Collin-Souffrin S., Hameury J.M., Joly M., 1988, A&A, 205, 19
Day C., Arnaud K., Ebisawa K., Gotthelf E., Ingham J., Mukai K., White N., 1995a, The ABC Guide to *ASCA* Data Reduction: version 4, NASA/GSFC
Day C., Jennings D., Seufert E., Watkins R., 1995b, *ASCA* Getting Started Guide for Revision 1 Data: version 4.1, NASA/GSFC
de Kool M., 1997, in Weymann R., Shlosman I., Arav N., eds, Mass Ejection from AGN. WSA Press, Pasadena, in press
Dotani T., Yamashita A., Rasmussen A., Team S., 1995, ASCA News, 3, 25
Dotani T., et al., 1996, ASCA News, 4, 3
Draine B.T., Salpeter E.E., 1979, ApJ, 231, 77
Fabian A.C., 1979, Proc. Roy. Soc. London A, 366, 449
Ferland G.J., 1992, University of Kentucky Department of Physics and Astronomy Internal Report
George I.M., Turner T.J., Netzer H., 1995, ApJ, 438, L67
Goodrich R.W., 1989, ApJ, 342, 224
Gotthelf E., 1996, *ASCA* News, 4, 31
Green P.J., Mathur S., 1996, ApJ, 462, 637
Joly M., 1993, Ann. Phys. Fr., 18, 241
Kolman M., Halpern J.P., Shrader C.R., Filippenko A.V., Fink H.H., Schaeidt S.G., 1993, ApJ, 402, 514
Lanzetta K.M., Turnshek D.A., Sandoval J., 1993, ApJS, 84, 109
Laor A., Draine B.T., 1993, ApJ, 402, 441
Laor A., Fiore F., Elvis M., Wilkes B.J., McDowell J.C., 1997, ApJ, 477, 93
Leighly K.M., Mushotzky R.F., Yaqoob T., Kunieda H., Edelson R., 1996, ApJ, 469, 14
Mathur S., Elvis M., Wilkes B.J., 1995, ApJ, 452, 230
Mathur S., Wilkes B.J., Aldcroft T., 1997, ApJ, 478, 182
Murphy E.M., Lockman F.J., Laor A., Elvis M., 1996, ApJS, 105, 369
Nandra K., George I.M., Mushotzky R.F., Turner T.J., Yaqoob T., 1997, ApJ, 477, 602
Osterbrock D.E., Pogge R.W., 1985, ApJ, 297, 166
Pounds K.A., Brandt W.N., 1997, in Makino F., Mitsuda K., eds, X-Ray Imaging and Spectroscopy of Cosmic Hot Plasmas: *ASCA* Third Anniversary Proceedings. Univ. Acad. Press, Tokyo, p. 209
Reynolds C.S., Fabian A.C., Nandra K., Inoue H., Kunieda H., Iwasawa K., 1995, MNRAS, 277, 901
Reynolds C.S., 1997, MNRAS, 286, 513
Shafer R.A., Haberl F., Arnaud K.A., Tennant A.F., 1991, XSPEC Users Guide. ESA Publications, Noordwijk
Shull J.M., Van Steenberg M., 1982, ApJS, 48, 95
Tanaka Y., Inoue H., Holt S.S., 1994, PASJ, 46, L37
Wills B.J., Wills D., Evans N.J., Natta A., Thompson K.L., Breger M., Sitko M.L., 1992, ApJ, 400, 96 (W92)

This paper has been produced using the Royal Astronomical Society/Blackwell Science LaTeX style file.